DNA Minor Groove Binding-Directed Poisoning of Human DNA Topoisomerase I by Terbenzimidazoles†

Zhitao Xu,‡ Tsai-Kun Li,§ Jung Sun Kim,|| Edmond J. LaVoie,||,⊥ Kenneth J. Breslauer,‡,⊥ Leroy F. Liu,§,⊥ and Daniel S. Pilch*,§,⊥

Department of Pharmacology, University of Medicine and Dentistry of New Jersey, Robert Wood Johnson Medical School, Piscataway, New Jersey 08854, Departments of Chemistry and Pharmaceutical Chemistry, Rutgers—The State University of New Jersey, Piscataway, New Jersey 08855, and The Cancer Institute of New Jersey, New Brunswick, New Jersey 08901

Received November 11, 1997; Revised Manuscript Received January 12, 1998

ABSTRACT: We have employed a broad range of spectroscopic, calorimetric, DNA cleavage, and DNA winding/unwinding measurements to characterize the DNA binding and topoisomerase I (TOP1) poisoning properties of three terbenzimidazole analogues, 5-phenylterbenzimidazole (5PTB), terbenzimidazole (TB), and 5-(naphthyl[2,3-*d*]imidazo-2-yl)bibenzimidazole (5NIBB), which differ with respect to the substitutions at their C5 and/or C6 positions. Our results reveal the following significant features. (i) The overall extent to which the three terbenzimidazole analogues poison human TOP1 follows the hierarchy 5PTB > TB ≫ 5NIBB. (ii) The impact of the three terbenzimidazole analogues on the superhelical state of plasmid DNA depends on the [total ligand] to [base pair] ratio (r_{bp}), having no effect on DNA superhelicity at r_{bp} ratios ≤0.1, while weakly unwinding DNA at r_{bp} ratios >0.1. This weak DNA unwinding activity exhibited by the three terbenzimidazoles does not appear to be correlated with the abilities of these compounds to poison TOP1. (iii) Upon complexation with both poly(dA)·poly(dT) and salmon testes DNA, the three terbenzimidazole analogues exhibit flow linear dichroism properties characteristic of a minor groove-directed mode of binding to these host DNA duplexes. (iv) The apparent minor groove binding affinities of the three terbenzimidazole analogues for the $d(GA_4T_4C)_2$ duplex follow a qualitatively similar hierarchy to that noted above for ligand-induced poisoning of human TOP1—namely, 5PTB > TB > 5NIBB. In the aggregate, our results suggest that DNA minor groove binding, but not DNA unwinding, is important in the poisoning of TOP1 by terbenzimidazoles.

DNA topoisomerase I (TOP1)[1] has become an attractive new molecular target for anticancer chemotherapeutic agents due, in large part, to the clinical development of the camptothecin family of compounds (*1*). Recent studies have shown that camptothecin binds to the TOP1−DNA interface (*2, 3*), while exhibiting little or no binding affinity for either the DNA or the enzyme alone (*2, 4*). Upon binding to the TOP1−DNA interface, camptothecin inhibits the religation step of the TOP1 reaction, thereby resulting in the accumulation of an enzyme−DNA−drug ternary cleavable complex (*4*−*6*). In addition to the camptothecins, the bibenzimidazoles (*7*−*10*) and the terbenzimidazoles (*11*) recently have been identified as poisons of human TOP1. However, the molecular mechanism(s) by which these TOP1-directed drugs achieve their biochemical/biological effects remains to be determined.

In contrast to the lack of DNA binding exhibited by camptothecin, crystallographic (*12*−*16*) and NMR (*17*−*19*) studies have revealed that both the bibenzimidazoles and the terbenzimidazoles bind to the minor groove of AT-tract duplex DNA, an observation suggesting that DNA minor groove binding may play a role in the poisoning of TOP1 by these compounds. However, this potential role has been obscured by the demonstration that selected bibenzimidazole and terbenzimidazole derivatives can unwind duplex DNA (*7, 8, 20*).

In an effort to define the role(s) that specific ligand−DNA interactions play in TOP1 poisoning, we have initiated studies to characterize and cross-correlate the DNA binding and TOP1 poisoning properties of various families of ligands. In this work, we employ spectroscopic, calorimetric, DNA cleavage, and DNA winding/unwinding measurements to characterize the TOP1 poisoning and DNA binding properties of three terbenzimidazole derivatives, 5-phenylterbenzimidazole (5PTB), terbenzimidazole (TB), and 5-(naphthyl[2,3-*d*]imidazo-2-yl)bibenzimidazole (5NIBB), which differ with

† This work was supported by National Institutes of Health Grants GM23509, GM34469, CA47995, and CA39962.

* Author to whom correspondence should be addressed at Department of Pharmacology, UMDNJ, Robert Wood Johnson Medical School, 675 Hoes Lane, Piscataway, NJ 08854-5635. Telephone: 732-445-3954. Fax: 732-445-5312. E-mail: pilch@rutchem.rutgers.edu.

‡ Rutgers University, Department of Chemistry.

§ UMDNJ, Robert Wood Johnson Medical School.

|| Rutgers University, Department of Pharmaceutical Chemistry.

⊥ Cancer Institute of New Jersey.

[1] Abbreviations: TOP1, topoisomerase I; 5PTB, 5-phenylterbenzimidazole; TB, terbenzimidazole; 5NIBB, 5-(naphthyl[2,3-*d*]imidazo-2-yl)bibenzimidazole; EtBr, ethidium bromide; Ho33342, Hoechst 33342; p(dA)·p(dT), poly(dA)·poly(dT); EDTA, disodium salt of ethylenediaminetetraacetic acid; SDS, sodium dodecyl sulfate; r_{bp}, [total ligand] to [base pair] ratio; r_{dup}, [total ligand] to [duplex] ratio; T_m, melting temperature; LD, linear dichroism; LD^r, reduced linear dichroism; ICD, induced circular dichroism; DSC, differential scanning calorimetry; UV−vis, ultraviolet−visible.

S0006-2960(97)02774-8 CCC: $15.00
Published on Web 02/20/1998

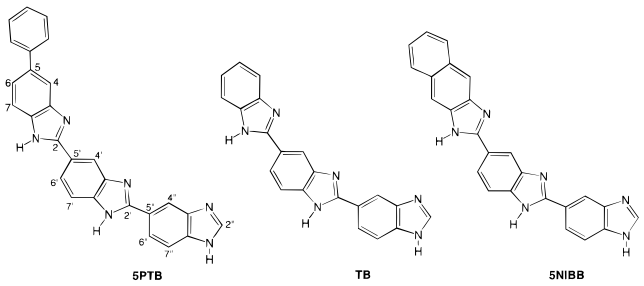

FIGURE 1: Chemical structures of 5-phenylterbenzimidazole (5PTB), terbenzimidazole (TB), and 5-(naphthyl[2,3-*d*]imidazo-2-yl)bibenzimidazole (5NIBB). The atomic numbering is indicated in the structure of 5PTB (left).

respect to the substituents at their C5 and/or C6 positions (see Figure 1). Our results suggest that DNA minor groove binding, but not DNA unwinding, is critical to the TOP1 poisoning capabilities of terbenzimidazoles.

MATERIALS AND METHODS

Enzyme, DNA, and Ligand Molecules. Recombinant human DNA TOP1 was isolated from *Escherichia coli* BL21(DE3) as described previously (*21*). Synthetic poly(dA)·poly(dT) [p(dA)·p(dT)] was obtained from Pharmacia Biotech, Inc. (Piscataway, NJ) and was used without further purification. The single-stranded d(GA_4T_4C) oligomer was synthesized on a BioSearch 8600 Synthesizer using standard cyanoethyl phosphoramidite chemistry, followed by purification using reverse phase HPLC. The molar extinction coefficient of d(GA_4T_4C) at 260 nm and 95 °C was determined by enzymatic digestion and subsequent phosphate analysis (*22*) to be 93 300 (mol strand/L)$^{-1}$ cm^{-1} in 10 mM sodium cacodylate (pH 7.0). 5-Phenylterbenzimidazole (5PTB), terbenzimidazole (TB), and 5-(naphthyl[2,3-*d*]-imidazo-2-yl)bibenzimidazole (5NIBB) were synthesized as described previously (*11*). Ethidium bromide (EtBr) and Hoechst 33342 (Ho33342) were obtained from Sigma Chemical Co. (St. Louis, MO). Both drugs were used without further purification.

Human TOP1 Cleavage Assay. Human TOP1 cleavage assays were conducted as previously reported (*4, 8*). Briefly, YEpG DNA was linearized with *Bam*HI and 3′-end-labeled with Klenow polymerase and [α-^{32}P]dCTP. Following phenol extraction and ethanol precipitation, the labeled DNA was resuspended in 10 mM Tris-HCl (pH 8.0) and 1 mM EDTA. The cleavage reaction mixtures (20 μL) contained 40 mM Tris-HCl (pH 8.0), 100 mM KCl, 10 mM $MgCl_2$, 0.5 mM dithiothreitol, 0.5 mM EDTA, 30 μg/mL bovine serum albumin, 10 ng of labeled YEpG DNA, and 5 ng of human DNA TOP1. The reaction mixtures were incubated at 23 °C for 15 min. The reactions then were terminated by addition of SDS and proteinase K to final concentrations of 1% and 200 μg/mL, respectively. Following addition of the SDS and proteinase K, the reaction mixtures were further incubated for 1 h at 37 °C, whereupon the DNA in each reaction mixture was alkali denatured by addition of NaOH, EDTA, sucrose, and bromophenol blue to final concentrations of 75 mN, 5 mM, 2.5%, and 0.04 mg/mL, respectively. The samples then were loaded onto a 1% agarose gel and electrophoresed at room temperature in a buffer containing 40 mM Tris-phosphate (pH 8.3) and 1 mM EDTA (0.5× TPE buffer).

DNA Unwinding Assay. The DNA unwinding assay was conducted in essentially the same manner as described previously (*8, 23*) using a mixture of supercoiled and relaxed pRS413 DNA (*24*) as substrates. A mixture of supercoiled and relaxed DNA was used in the unwinding assay to ensure that TOP1 catalyzed complete relaxation of the DNA, which is revealed by a single Gaussian distribution of topoisomers rather than two separate Gaussian distributions. Initially, reaction mixtures (20 μL) contained 40 mM Tris-HCl (pH 8.0), 100 mM KCl, 10 mM $MgCl_2$, 0.5 mM dithiothreitol, 0.5 mM EDTA, 30 μg/mL bovine serum albumin, 0.3 μg of DNA, and 0−250 μM ligand. Upon complete mixing of these reaction components, human TOP1 (5 ng) was added to the reaction mixture, which then was incubated at 37 °C for 15 min. The reactions were terminated by addition of SDS and EDTA to final concentrations of 1% and 50 mM, respectively. Following phenol extraction, sucrose and bromophenol blue were added to final concentrations of 4% and 0.04 mg/mL, respectively. The samples then were loaded onto a 1% agarose gel and electrophoresed at room temperature in 0.5× TPE buffer.

UV−Vis Spectrophotometry. All UV−vis absorbance experiments were conducted on an AVIV Model 14DS Spectrophotometer (Aviv Associates, Lakewood, NJ) equipped with a thermoelectrically controlled cell holder. A quartz cell with a 1 cm path length was used for all the absorbance studies. Isothermal (25 °C) absorption spectra for the linear dichroism experiments were acquired from 240 to 440 nm. The poly(dA)·poly(dT) solutions were 50 μM in base pair and contained 10 mM sodium phosphate (pH 6.8), 100 mM NaCl, 0.1 mM EDTA, and 5PTB, TB, or 5NIBB at a concentration of 0 or 5 μM.

Absorbance versus temperature profiles were measured at 260 nm in CMKE buffer [10 mM sodium cacodylate (pH 6.8), 10 mM $MgCl_2$, 100 mM KCl, and 1 mM EDTA] with a 6 s averaging time. The temperature was raised in 0.5 °C increments, and the samples were allowed to equilibrate for 1 min at each temperature setting. For each optically detected transition, the melting temperature (T_m) was determined as previously described (*25*). The d(GA_4T_4C)$_2$ concentration was 2 μM in duplex, while the ligand concentrations ranged from 0 to 4 μM.

Flow Linear Dichroism (LD) Measurements. Flow linear dichroism measurements were conducted as previously described (*26*). Each flow linear dichroism spectrum shown in Figure 4 was acquired from 240 to 440 nm and reflects the average of two scans. A Couette cell with a total optical path length of 1.2 mm was used for all the linear dichroism studies. The poly(dA)·poly(dT) solutions were 50 μM in base pair and contained 10 mM sodium phosphate (pH 6.8), 100 mM NaCl, 0.1 mM EDTA, and 5PTB, TB, or 5NIBB at a concentration of 0 or 5 μM.

Isothermal, Stopped-Flow Mixing Microcalorimetry. Isothermal calorimetric measurements were performed at 20 °C using an all-tantalum, differential, stopped-flow, heat conduction microcalorimeter (model DSFC-100; Commonwealth Technology, Inc., Alexandria, VA) developed by Mudd and Berger (*27, 28*). In a typical experiment, the reaction is initiated by a microprocessor-controlled stepping motor that activates a syringe drive which delivers, within 0.6 s, 80 μL of each reagent [16 μM in duplex d(GA_4T_4C)$_2$ and 16 μM ligand] into tantalum mixing chambers, with distilled water

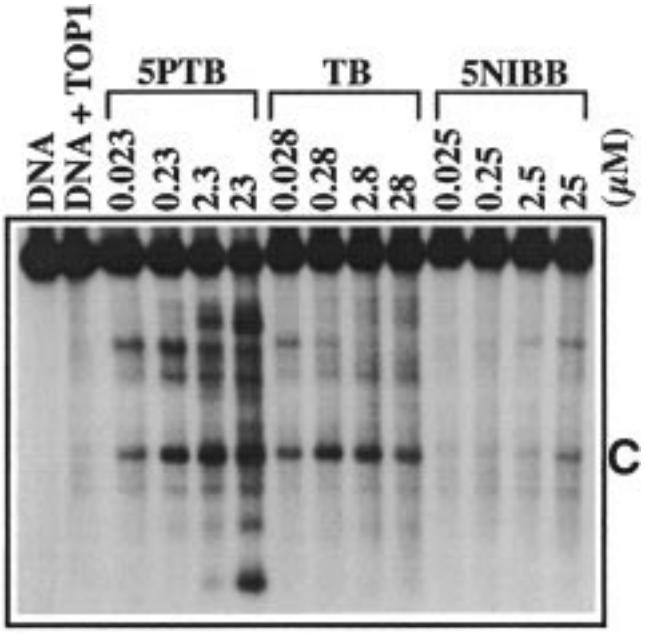

FIGURE 2: Agarose gel showing TOP1-mediated DNA cleavage in the presence of the three terbenzimidazole derivatives. The ligands and their concentrations are indicated at the tops of the lanes. The band labeled C corresponds to the band C cleavage product induced by Ho33342, as reported previously by the Liu group (*7, 8*).

being used in the reference mixing chamber. A delay of 300 s was used between each injection/reaction. Each reaction generated a heat burst curve (μJ/s vs s), with the area under the curve being determined by integration to obtain the heat for that reaction. Ligand−$d(GA_4T_4C)_2$ mixing heats were 59, 33, and 56 μJ for 5PTB, TB, and 5NIBB, respectively. When compared with the corresponding ligand−buffer mixing heats of 32, 23, and 46 μJ, these data reflect signal-to-noise ratios ranging from 1.2 to 1.8. No significant integral heat of dilution was observed for the $d(GA_4T_4C)_2$ duplex. The calorimeter was calibrated chemically by measuring the heat associated with a 1:2 dilution of 10 mM NaCl (*29, 30*). The enthalpy of ligand binding to the $d(GA_4T_4C)_2$ duplex was determined by dividing the measured heat for each reaction by the concentration of bound ligand. When necessary, the appropriate correction for the concentration of bound ligand was deduced from induced circular dichroism (ICD) equilibrium binding data (not shown).

RESULTS AND DISCUSSION

The Overall Extent to Which the Three Terbenzimidazole Derivatives Stimulate Human TOP1-Mediated DNA Cleavage Follows the Hierarchy 5PTB > TB ≫ 5NIBB. We compared the abilities of 5PTB, TB, and 5NIBB to poison human TOP1 by measuring the relative extents to which they stimulate TOP1-mediated DNA cleavage. The resulting cleavage patterns are shown in Figure 2. Inspection of Figure 2 reveals that the three terbenzimidazole analogues stimulate TOP1-mediated DNA cleavage in a concentration-dependent manner, with the overall extent to which they stimulate cleavage following the hierarchy 5PTB > TB ≫ 5NIBB. Further inspection of Figure 2 reveals that this hierarchy of ligand-induced cleavage does not apply to all of the observed cleavage products. For example, the extent to which 5PTB and TB stimulate TOP1-mediated cleavage at the site corresponding to band C is similar, with this extent of induced cleavage being substantially greater than that induced by 5NIBB. Thus, in contrast to the hierarchy of overall ligand-induced cleavage noted above, the stimulation of TOP1-mediated cleavage at the site corresponding to band C follows the hierarchy 5PTB ≈ TB ≫ 5NIBB. This heterogeneity in ligand-induced cleavage may reflect differences in the base sequence specificities with which the three terbenzimidazole derivatives bind to duplex DNA.

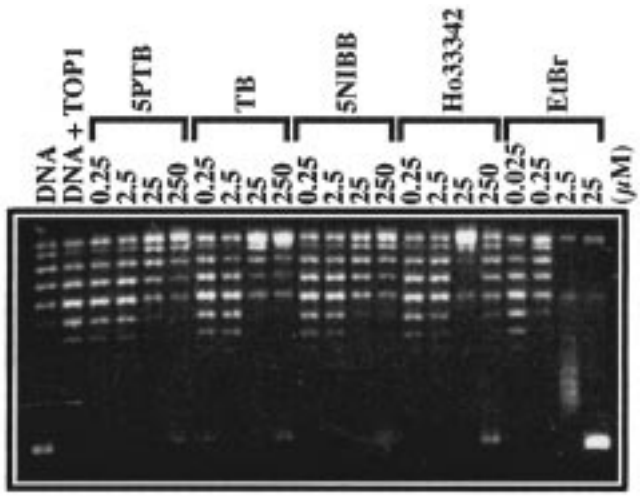

FIGURE 3: Agarose gel showing the extent of DNA duplex unwinding by increasing concentrations of 5PTB, TB, 5NIBB, ethidium bromide (EtBr), and Hoechst 33342 (Ho33342) in the presence of human TOP1. The ligands and their concentrations are indicated at the tops of the lanes.

Stimulation of TOP1-Mediated DNA Cleavage by the Three Terbenzimidazole Analogues Is Not a Result of Ligand-Induced DNA Unwinding. DNA unwinding measurements were conducted to assess the impact, if any, of 5PTB, TB, and 5NIBB on the superhelical state of circular duplex DNA. The resulting unwinding profiles are shown in Figure 3. As a positive control for classical intercalation, Figure 3 also shows the DNA unwinding profile for ethidium bromide (EtBr). In these experiments, ligand-induced DNA unwinding is revealed by an upward and subsequent downward shift in the mobilities of the Gaussian distributions of topoisomers as a function of increasing ligand concentration. Inspection of Figure 3 reveals that, at ligand concentrations ≤ 2.5 μM (r_{bp} ratios ≤ 0.1), none of the three terbenzimidazole analogues unwinds duplex DNA, an observation consistent with a minor groove-directed mode of DNA binding. In fact, as described in the next section, 5PTB, TB, and 5NIBB also exhibit linear dichroism properties characteristic of minor groove-directed DNA binding. Further inspection of Figure 3 reveals that, at ligand concentrations > 2.5 μM (r_{bp} ratios > 0.1), each of the three terbenzimidazole derivatives induces a small degree of DNA unwinding. This observation may reflect a secondary DNA binding mode which results in a small degree of unwinding, a "dual-mode" DNA binding behavior we previously have reported in spectroscopic and viscometric studies on 5PTB (*20*). Note that the extents to which high concentrations of the terbenzimidazoles unwind DNA are substantially smaller in magnitude than the corresponding degree of unwinding induced by similar concentrations of the classic intercalator EtBr. Thus, it is unlikely

that the secondary DNA binding behavior exhibited by the terbenzimidazoles is intercalative in nature. In addition, none of the three terbenzimidazoles differ in the extent to which they unwind DNA. By contrast, as noted above, these ligands exhibit substantially different abilities to stimulate TOP1-mediated DNA cleavage. Thus, the small degree of DNA unwinding induced by high concentrations of the three terbenzimidazoles studied here do not correlate with the extents to which these ligands poison TOP1. In other words, the secondary DNA binding mode that results in a small degree of DNA unwinding is not essential to the TOP1 poisoning capabilities of the terbenzimidazole derivatives.

The Liu group previously has identified the bibenzimidazoles Hoechst 33258 (Ho33258) and Ho33342 as potent TOP1 poisons (*7, 8*). NMR and crystallographic studies have revealed that these ligands bind to the minor groove of AT-tracts in duplex DNA (*12*−*15, 18, 19*). However, Liu and co-workers have shown that high concentrations of these ligands induce DNA unwinding (*7, 8*). This latter observation has hindered identification of the molecular basis for the TOP1 poisoning activities of Ho33258 and Ho33342. To alleviate this situation, we compared the DNA unwinding profile of Ho33342 with those of the three terbenzimidazoles (see Figure 3). Note that Ho33342 behaves similarly to the terbenzimidazoles in exhibiting DNA unwinding activity only at concentrations >2.5 μM (r_{bp} ratios >0.1), although the extent to which Ho33342 unwinds DNA is greater than that induced by any of the terbenzimidazoles. The same dual-mode DNA binding model invoked above for the terbenzimidazoles also can be invoked here for Ho33342. Thus, it is reasonable to propose, by extension, that, like the terbenzimidazoles, the DNA unwinding properties of Ho33342 are not the important factors in determining its TOP1 poisoning capability.

All Three Terbenzimidazole Analogues Exhibit Linear Dichroism Properties Characteristic of a Minor Groove-Directed Mode of DNA Binding. Flow linear dichroism is a useful technique for defining the mode by which a ligand is complexed with a host nucleic acid structure (*31, 32*). Linear dichroism (LD) is defined by the relationship

$$\mathrm{LD} = A_{\parallel} - A_{\perp} \tag{1}$$

where $A_{\parallel}$ and $A_{\perp}$ denote, respectively, the sample absorbances with the polarization vectors of the light oriented either in a parallel or a perpendicular orientation with respect to the flow lines. When the transition dipole moment of a singly oriented chromophore (e.g., a DNA base and/or a bound aromatic ligand) lies within the plane of the molecule and makes an angle, θ, with the orientation axis, this angle can be related to the value of the reduced LD ($\mathrm{LD^r}$) by the equation (*26, 31*−*33*)

$$\mathrm{LD^r} = \frac{\mathrm{LD}}{A} = \frac{3}{2}(3\cos^2\theta - 1)[F(G)] \tag{2}$$

where A is the isotropic absorbance of the sample and $F(G)$ is an orientation factor, which has values in the range of $0 < F(G) < 1$, and is a function of the velocity gradient G, the extent of deformation of the nucleic acid molecule in the flow field, and an average of the projections of the axes of the partially oriented local DNA segments onto the laboratory axes. Equation 2 implies that a positive $\mathrm{LD^r}$ signal is associated with an orientation angle θ of <55°, while a negative $\mathrm{LD^r}$ signal is associated with an orientation angle θ of >55°. In a typical flow LD experiment, the long axis of the nucleic acid helix is aligned along the flow lines (*26, 31*−*33*). Thus, the nucleic acid bases, which are oriented roughly perpendicular to the helix axis (i.e., $\theta_{bases} \approx 90°$), give rise to a negative $\mathrm{LD^r}$ signal. A ligand molecule that is bound to the minor groove of a nucleic acid structure typically exhibits an orientation angle, $\theta_{lig,}$ of approximately 25−40° relative to the helix axis, and therefore gives rise to a positive $\mathrm{LD^r}$ signal. In contrast to a minor groove-bound ligand molecule, an intercalated ligand molecule, like the nucleic acid bases, is oriented roughly perpendicular to the helix axis ($\theta_{lig} \approx 90°$), and therefore gives rise to a negative $\mathrm{LD^r}$ signal. An estimate of the average ligand orientation angle (θ_{lig}) in a ligand−nucleic acid complex can be derived from the $\mathrm{LD^r}$ values of the nucleic acid alone [$(\mathrm{LD^r})_{NA}$] and its ligand complex [$(\mathrm{LD^r})_{lig-NA}$] using the following relationship (*34*):

$$\frac{(\mathrm{LD^r})_{lig-NA}}{(\mathrm{LD^r})_{NA}} = 1 - 3\cos^3(\theta_{lig}) \tag{3}$$

Figure 4 shows the absorbance (tops of panels A−C) and LD (bottoms of panels A−C) spectra of the p(dA)·p(dT) duplex and its complex with either 5PTB (panel A), TB (panel B), or 5NIBB (panel C) at a [total ligand]/[base pair] ratio (r_{bp}) of 0.1. Inspection of Figure 4 reveals that, as expected, the LD spectra of p(dA)·p(dT) alone, as well as of the three ligand−p(dA)·p(dT) complexes, are negative in the 240−300 nm wavelength region where the DNA bases absorb. By contrast, the LD spectra of the three ligand−p(dA)·p(dT) complexes are positive in the 320−370 nm ligand-absorbing wavelength region. These positive LD signals are due to the effects of ligand−DNA complexation, since the LD spectrum of p(dA)·p(dT) alone is essentially zero in the 320−370 nm wavelength region. Furthermore, these positive LD signals indicate that the average orientation angles (θ_{lig}) of the three terbenzimidazoles in their complexes with p(dA)·p(dT) are <55°.

As a first step toward estimating values for θ_{lig} in the three terbenzimidazole−p(dA)·p(dT) complexes, we derived $\mathrm{LD^r}$ spectra for p(dA)·p(dT) and its terbenzimidazole complexes by dividing the absorption spectra shown in Figure 4 (top panels) by the corresponding LD spectra (Figure 4, bottom panels). The resulting $\mathrm{LD^r}$ spectra are shown in Figure 5. Note that the positive $\mathrm{LD^r}$ signals of the 5PTB−p(dA)·p(dT) (Figure 5A), TB−p(dA)·p(dT) (Figure 5B), and 5NIBB−p(dA)·p(dT) (Figure 5C) complexes in the ligand-absorbing 325−360 nm region are, within experimental error, essentially constant with wavelength. This observation suggests that the transition moments of all the p(dA)·p(dT)-bound ligand molecules in these complexes are similarly oriented.

Table 1 summarizes the $\mathrm{LD^r}$ values derived from the $\mathrm{LD^r}$ spectra in Figure 5 at wavelengths which correspond to the appropriate LD minima or maxima (see Figure 4) of p(dA)·p(dT) alone and its terbenzimidazole complexes. Armed with these $\mathrm{LD^r}$ values, we used eq 3 to calculate θ_{lig} in each of the terbenzimidazole−p(dA)·p(dT) complexes. The resulting θ_{lig} values are listed in Table 1. Inspection of these data

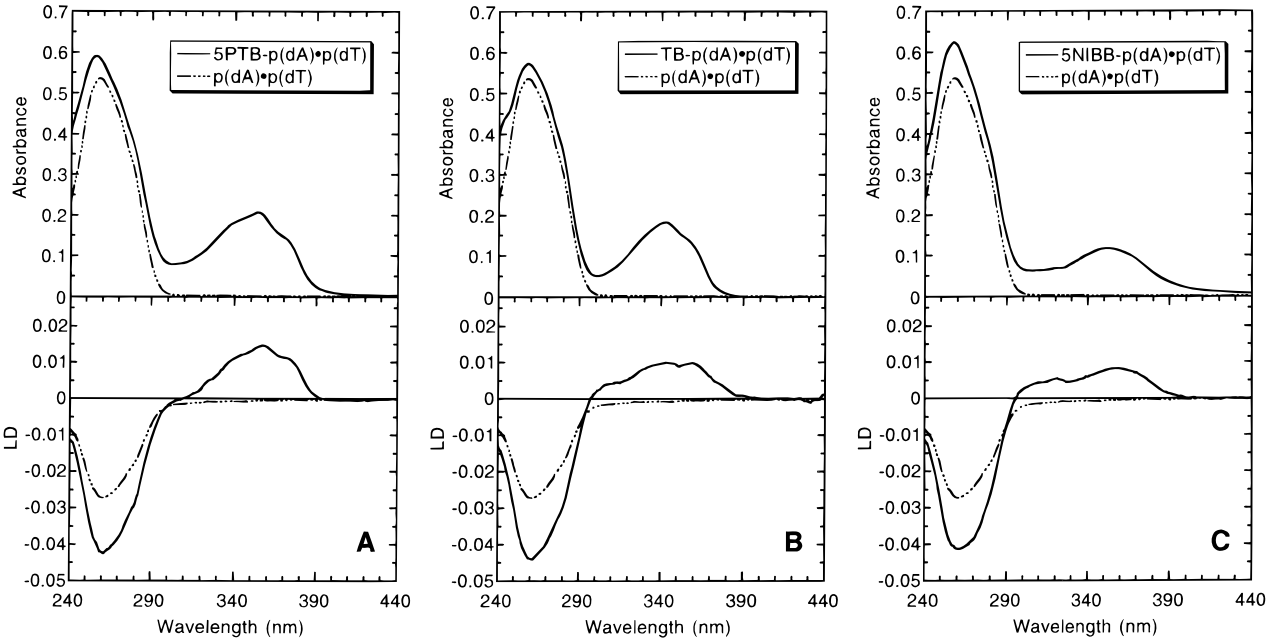

FIGURE 4: Isothermal absorbance and linear dichroism (LD) spectra at 25 °C of p(dA)·p(dT) and its complexes with 5PTB (A), TB (B), and 5NIBB (C) at a [total ligand] to [base pair] ratio (r_{bp}) of 0.1. Solution conditions are 10 mM sodium phosphate (pH 6.8), 100 mM NaCl, and 0.1 mM EDTA.

reveals that the p(dA)·p(dT)-bound 5PTB, TB, and 5NIBB molecules make, respectively, angles of 27°, 34°, and 27° with the DNA helical axis. These values of θ_{lig} are consistent with the binding of 5PTB, TB, and 5NIBB to the minor groove of the poly(dA)·poly(dT) duplex, an observation in agreement with a recent crystallographic study by Neidle and co-workers (*16*), which revealed the minor groove-directed binding of a terbenzimidazole analogue of Ho33258 (TRIBIZ) to the $d(CGCA_3T_3GCG)_2$ host duplex. Note that 5PTB, TB, and 5NIBB also exhibit similar LD behaviors when complexed with salmon testes DNA (not shown). Hence, these LD properties are not unique to terbenzimidazole−p(dA)·p(dT) complexes.

In the sections that follow, we describe the use of spectroscopic and calorimetric techniques to characterize the relative DNA binding strengths of 5PTB, TB, and 5NIBB. The $d(GA_4T_4C)_2$ duplex was chosen as the DNA target in these studies, since our previous studies (*35*) have shown that 5PTB exhibits a high binding affinity for this duplex.

The Three Terbenzimidazole Analogues Bind to the $d(GA_4T_4C)_2$ Duplex and Enhance Its Thermal Stability. Panels A−C of Figure 6 show the UV melting curves for the $d(GA_4T_4C)_2$ duplex in the absence and presence of increasing amounts of 5PTB (panel A), TB (panel B), or 5NIBB (panel C). Note that as one increases the [total ligand] to [duplex] ratio (r_{dup}), the thermal stability of the $d(GA_4T_4C)_2$ duplex increases, with r_{dup} ratios higher than those shown having little or no effect on the melting temperature (T_m) of the host duplex. These ligand-induced changes in duplex thermal stability are consistent with all three ligands binding to the target duplex, with a preference for the duplex versus single-stranded state (*36, 37*). Further inspection of Figure 6 reveals that the maximal extent of ligand-induced enhancement in duplex thermal stability (ΔT_m), defined as the duplex T_m in the presence of saturating concentrations of ligand minus the duplex T_m in the absence of ligand, follows the hierarchy 5PTB > TB > 5NIBB. Specifically, the maximal extents to which the binding of 5PTB, TB, and 5NIBB increase the thermal stability of the $d(GA_4T_4C)_2$ duplex are approximately 19, 13, and 8 °C, respectively. In the section that follows, we describe how these ligand-induced changes in duplex thermal stability can be used to estimate apparent ligand−duplex association constants.

5PTB, TB, and 5NIBB Binding Affinities for the $d(GA_4T_4C)_2$ Duplex Derived from UV Melting Data. To assess, by a single method, the relative strength of 5PTB, TB, and 5NIBB binding to the $d(GA_4T_4C)_2$ duplex, we used a ΔT_m approach previously described in detail (*36*) and briefly summarized below. Significantly, we previously have employed this ΔT_m method successfully to determine ligand binding affinities for both oligomeric and polymeric host duplexes (*37*−*41*). It should be noted that the magnitude of 5PTB, TB, and 5NIBB binding to the $d(GA_4T_4C)_2$ duplex, as well as the presence of competing ligand self-association equilibria, precludes a Scatchard analysis of optical (e.g., absorbance or ICD) titration data. Consequently, to calculate ligand binding affinities, we used the Crothers ΔT_m approach (*36*) described below, which considers only differences between the ligand-free and ligand-saturated duplexes, and therefore is not compromised by the nature of the aggregation state of the free ligand.

We used our measured, maximal, ligand-induced changes in the thermal stability (ΔT_m) of the $d(GA_4T_4C)_2$ duplex (see Figure 6 and Table 2) to estimate apparent ligand binding constants at T_m (K_{T_m}) from the expression (*36*):

$$\frac{1}{T_m^\circ} - \frac{1}{T_m} = \frac{nR}{(\Delta H_{dup})} \ln[1 + (K_{T_m})L_f] \qquad (4)$$

where T_m° and T_m are, respectively, the duplex melting temperatures in the absence and presence of ligand at duplex-saturating r_{dup} ratios; n is the number of ligand binding sites on the duplex; ΔH_{dup} is the enthalpy change for the melting

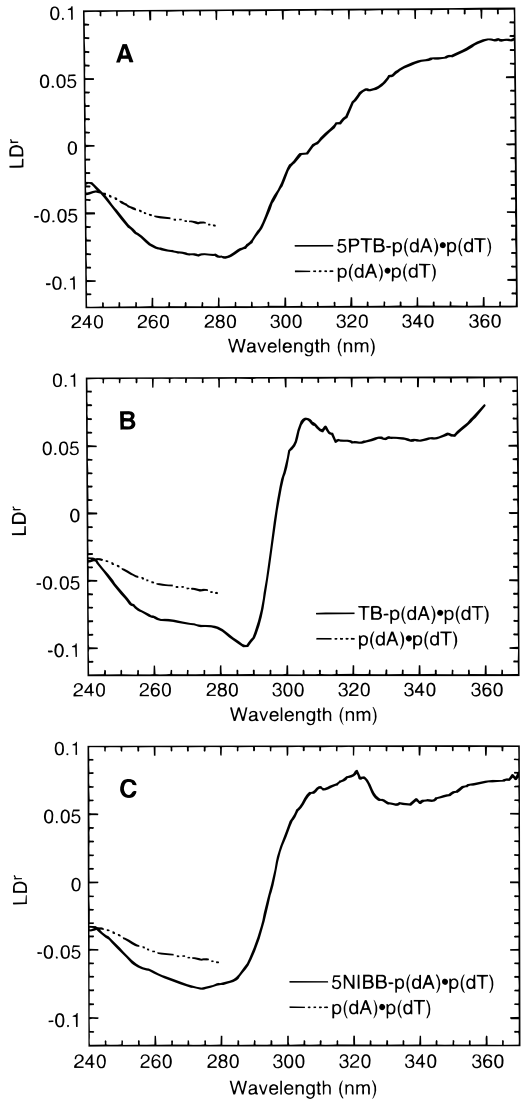

FIGURE 5: Reduced linear dichroism (LD^r) spectra at 25 °C of p(dA)·p(dT) and its complexes with 5PTB (A), TB (B), and 5NIBB (C) at a [total ligand] to [base pair] ratio (r_{bp}) of 0.1. Solution conditions are as described in the legend to Figure 4.

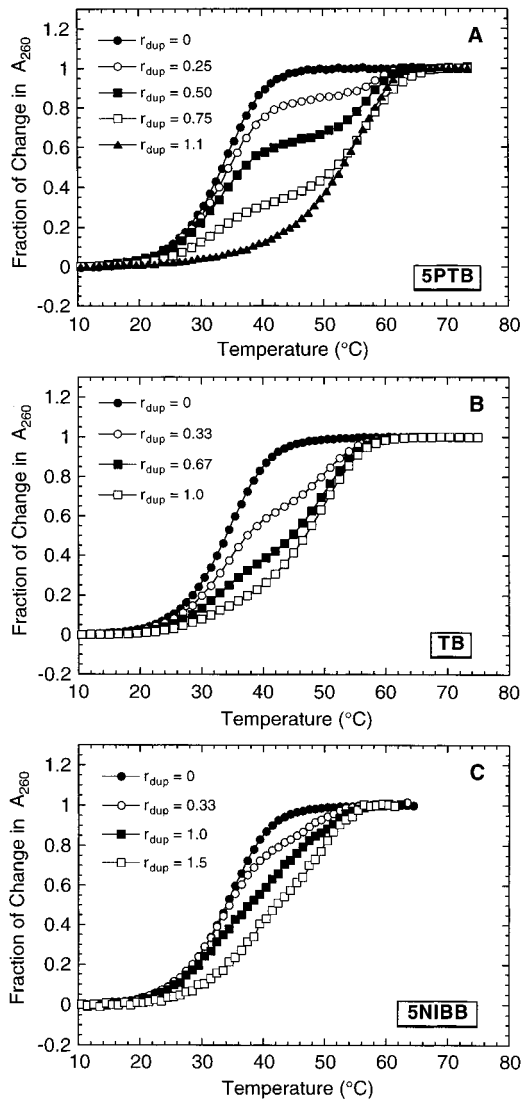

FIGURE 6: UV melting profiles for the $d(GA_4T_4C)_2$ duplex and its complexes with 5PTB (A), TB (B), and 5NIBB (C) at the indicated [total ligand] to [duplex] ratios (r_{dup}). Solution conditions are 10 mM sodium cacodylate (pH 6.8), 10 mM $MgCl_2$, 100 mM KCl, and 1 mM EDTA. For clarity of presentation, the melting profiles are cast plots of fractional change in absorbance at 260 nm (A_{260}) versus temperature, as obtained by subtraction of the upper and lower baselines (*25*).

Table 1: Reduced Linear Dichroism (LD^r) Values and Average Ligand Orientation Angles (θ_{lig}) for p(dA)·p(dT) and/or Its Complexes with 5PTB, TB, and 5NIBB[a]

sample	wavelength (nm)	LD^r	θ_{lig} (deg)[b]
p(dA)·p(dT)	261	−0.052	na
5PTB-p(dA)·p(dT)	357	+0.073	27
TB-p(dA)·p(dT)	343	+0.055	34
5NIBB-p(dA)·p(dT)	355	+0.071	27

[a] Solution conditions are 10 mM sodium cacodylate (pH 6.8), 100 mM NaCl, and 0.1 mM EDTA. [b] Values of θ_{lig} for each of the ligand−p(dA)·p(dT) complexes were determined using eq 3. The abbreviation na denotes not applicable.

of the DNA duplex in the absence of bound ligand [a value we determined previously using DSC (*35*)]; and L_f is the free ligand concentration at T_m. For the tightly bound $d(GA_4T_4C)_2$ complexes with 5PTB and TB, we estimated L_f as one-half the total ligand concentration (L_{tot}) whereas, for the more weakly bound 5NIBB−$d(GA_4T_4C)_2$ complex, we estimated L_f as L_{tot} minus one-half the total duplex concentration. We then extrapolated the K_{T_m} values calculated in this manner to a common reference temperature of 20 °C using the standard thermodynamic relationship

$$\frac{\partial(\ln K)}{\partial(1/T)} = -\frac{\Delta H_b}{R} \quad (5)$$

where ΔH_b is the enthalpy of ligand binding.

Apparent Binding Affinities of the Three Terbenzimidazole Derivatives for the $d(GA_4T_4C)_2$ Duplex Follow the Hierarchy 5PTB > TB > 5NIBB. Table 2 summarizes the apparent association constants at 20 °C (K_{20}) that we have calculated using eqs 4 and 5, for 5PTB, TB, and 5NIBB binding to the $d(GA_4T_4C)_2$ host duplex. The 5PTB, TB, and 5NIBB binding enthalpies required for extrapolation of the binding constants at T_m to a common reference temperature of 20 °C using eq 5 were determined using isothermal, stopped-flow mixing calorimetry. Figure 7 shows representative heat burst curves for the binding of 5PTB (panel A), TB (panel B), and 5NIBB (panel C) to the $d(GA_4T_4C)_2$ duplex. The

Table 2: ΔT_m-Derived Binding Affinities of 5PTB, TB, and 5NIBB for the $d(GA_4T_4C)_2$ Duplex at 20 °C[a]

ligand	$T_m°$ [b] (°C)	T_m [b] (°C)	K_{20} [c] (M^{-1})
5PTB	34.1 ± 0.1	53.3 ± 0.2	$(8.9 \pm 2.4) \times 10^9$
TB	34.1 ± 0.1	47.0 ± 0.2	$(3.9 \pm 0.7) \times 10^8$
5NIBB	34.1 ± 0.1	42.3 ± 0.3	$(2.6 \pm 0.6) \times 10^7$

[a] Solution conditions are 10 mM sodium cacodylate (pH 6.8), 10 mM $MgCl_2$, 100 mM KCl, and 1 mM EDTA. [b] T_m values were derived from UV melting profiles at 2 μM duplex in the absence ($T_m°$) and presence of ligand at duplex−saturating r_{dup} ratios (1.1 for 5PTB, 1.0 for TB, and 1.5 for 5NIBB). Each T_m value is an average derived from at least two independent experiments, with the indicated errors corresponding to the standard deviation from the mean. [c] Binding constants at 20 °C (K_{20}) were determined using eqs 4 and 5, the appropriate values of ΔH_b listed in Table 3, and the calorimetrically determined duplex-to−single strand transition enthalpy (ΔH_{dup}) of 86.4 kcal/mol for $d(GA_4T_4C)_2$ (*35*). The indicated uncertainties reflect the maximum errors in K_{20} that result from the corresponding uncertainties in T_m, $T_m°$, and ΔH_b, as propagated through eqs 4 and 5.

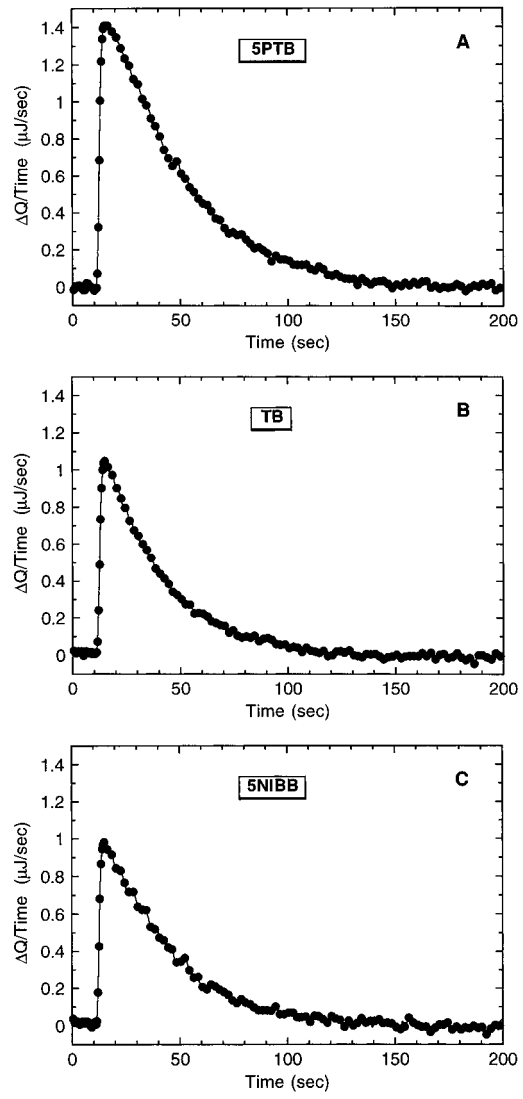

FIGURE 7: Isothermal, stopped-flow calorimetric heat burst curves at 20 °C for the complexation of $d(GA_4T_4C)_2$ with 5PTB (A), TB (B), and 5NIBB (C). Solution conditions are as described in the legend to Figure 6.

areas under these heat burst curves were determined by integration to yield the heats of the binding reactions. The resulting ΔH_b values are listed in Table 3. Inspection of these data reveals that the $d(GA_4T_4C)_2$ binding enthalpies of all three ligands are exothermic, with the 5PTB and 5NIBB binding enthalpies (−4.9 and −2.5 kcal/mol, respectively) being more exothermic (favorable) than the corresponding TB binding enthalpy (−1.8 kcal/mol). Note that 5PTB and 5NIBB differ from TB in that they contain an additional phenyl ring (see Figure 1). This additional phenyl ring may be engaged in favorable van der Waals interactions with DNA atoms lining the walls and/or floor of the minor groove, thereby giving rise to the enhanced enthalpic stabilities of the 5PTB−$d(GA_4T_4C)_2$ and 5NIBB−$d(GA_4T_4C)_2$ complexes relative to that of the corresponding TB−$d(GA_4T_4C)_2$ complex. The stabilizing influence of such ligand−DNA van der Waals contacts has previously been demonstrated in recent crystallographic studies on the complexes of the bibenzimidazole, Ho33258 (*12*−*15*), and the terbenzimidazole, TRIBIZ (*16*), with duplex DNA. Note that, while the binding of both 5PTB and 5NIBB to the $d(GA_4T_4C)_2$ duplex is more exothermic than the binding of TB, the extent of this enhancement in binding enthalpy ($\Delta\Delta H_b$) is 2.4 kcal/mol greater for 5PTB than for 5NIBB. This difference in $\Delta\Delta H_b$ may be due to a corresponding difference in range of motion between the *appended* phenyl ring of 5PTB and the *fused* phenyl ring of 5NIBB (see Figure 1). The appended phenyl ring of 5PTB is able to rotate freely about the bond through which it is linked to the 5-position of the terbenzimidazole, an ability that may facilitate the positioning of the ring for favorable van der Waals contacts with the minor groove of the host DNA duplex. By contrast, the fused phenyl ring of 5NIBB is not able to rotate independently of the benzimidazole moiety to which it is fused, and thereby may be constrained in its ability to achieve the proper positioning for maximization of van der Waals contacts with the host DNA.

Table 3: Calorimetrically-Derived Binding Enthalpies (ΔH_b) for the Interactions of 5PTB, TB, and 5NIBB with $d(GA_4T_4C)_2$ at 20 °C[a]

ligand	ΔH [b] (kcal/mol)
5PTB	−4.9 ± 0.6
TB	−1.8 ± 0.2
5NIBB	−2.5 ± 0.3

[a] Solution conditions are as described in the footnote to Table 2. [b] ΔH_b values were determined at a [total ligand] to [duplex] ratio (r_{dup}) of 1.0, with the indicated uncertainties corresponding to the sum of the standard errors from two separate mixing experiments (ligand−DNA and ligand−buffer) of at least 14 independent injections each.

Inspection of the data in Table 2 reveals that the apparent binding affinities for the $d(GA_4T_4C)_2$ duplex at 20 °C (K_{20}) follow the hierarchy 5PTB > TB > 5NIBB. Note the agreement between this hierarchy of apparent binding affinity and that defined above for binding-induced enhancement in duplex thermal stability. Thus, given the binding enthalpies listed in Table 2, the relative extent to which any one of the three terbenzimidazole derivatives thermally stabilizes the host $d(GA_4T_4C)_2$ duplex is correlated with its relative binding affinity.

DNA Minor Groove Binding Is Important in the Poisoning of TOP1 by Terbenzimidazole Derivatives. Crystallographic studies by the Neidle group (*16*) on the TRIBIZ−$d(CGCA_3T_3GCG)_2$ complex as well as our LD studies noted above on the three terbenzimidazole−p(dA)·p(dT) complexes are consistent in revealing the minor groove binding of terben-

zimidazoles to AT-tracts in duplex DNA. Hence, it is reasonable to propose, by extension, that 5PTB, TB, and 5NIBB also bind to the minor groove of the $d(GA_4T_4C)_2$ duplex. Furthermore, a comparison of our DNA binding affinity (Table 2) and DNA cleavage (Figure 2) data reveals that both the apparent $d(GA_4T_4C)_2$ binding affinities and the overall TOP1 poisoning activities of the terbenzimidazoles follow a similar hierarchy—namely, 5PTB > TB > 5NIBB. In the aggregate, these observations suggest that the strength of DNA minor groove binding by terbenzimidazole derivatives is correlated with the extent to which these ligands poison TOP1. In other words, DNA minor groove binding is important in the poisoning of TOP1 by terbenzimidazoles. Recently, we reported that minor groove-directed ligand−DNA interactions also appear to be involved in the poisoning of TOP1 by protoberberine analogues (*42*). Hence, ligand interaction(s) with the minor groove of the host DNA duplex may be of general importance in the poisoning of TOP1.

Molecular Basis for the Correlation between Minor Groove-Directed Ligand−DNA Interactions and TOP1 Poisoning. The work presented here contributes to an expanding database that underscores the importance of minor groove-directed ligand−DNA interactions in TOP1 poisoning. However, the molecular mechanism of TOP1 poisoning via ligand−minor groove interactions is unclear. Liu and co-workers have shown that minor groove binding alone, while necessary, is not sufficient for the poisoning of TOP1 by minor groove-directed ligands (*7*). Thus, both drug−DNA and drug−enzyme interactions may play roles in the stabilization of TOP−DNA−drug ternary cleavable complexes. Recently, we reported that 5PTB preferentially binds the $d(GA_4T_4C)_2$ duplex, which exhibits electrophoretic properties characteristic of "bent" DNA (i.e., anomalously slow gel migration), relative to the sequence isomeric $d(GT_4A_4C)_2$ duplex, which exhibits "normal" electrophoretic migration (*35*). In addition, we found that the electrophoretic behaviors of the 5PTB-free and 5PTB-bound duplexes were consistent with ligand-induced bending of both duplexes, which, for the $d(GA_4T_4C)_2$ duplex, was synergistic with the endogenous sequence-directed electrophoretic properties of the ligand-free duplex state (*35*). These observations suggest that TOP1 poisoning by minor groove-directed ligands may correlate with ligand-induced DNA bending. Two recent studies (*43, 44*) have demonstrated that bent DNA enhances TOP1 binding and catalysis, while also stimulating TOP1-mediated cleavage. Thus, by contrast with camptothecin, which poisons TOP1 by inhibiting the religation step of the enzyme reaction (*4*−*6*), minor groove binding ligands may poison TOP1 by stabilizing a bent DNA conformation, which, in turn, stimulates the DNA binding of the enzyme. Clearly, additional studies are required to further define the role(s) of specific ligand−DNA interactions in TOP1 poisoning.

ACKNOWLEDGMENT

We are indebted to Mr. Chiang Yu for his assistance with the TOP1 cleavage assays.

REFERENCES

1. Potmesil, M., and Pinedo, H. (1995) *Camptothecins: New Anticancer Agents*, CRC Press, Boca Raton, FL.
2. Hertzberg, R. P., Busby, R. W., Caranfa, M. J., Holden, K. G., Johnson, R. K., Hecht, S. M., and Kingsbury, W. D. (1990) *J. Biol. Chem. 265*, 19287−19295.
3. Pommier, Y., Kohlhagen, G., Kohn, K. W., Leteurtre, F., Wani, M. C., and Wall, M. E. (1995) *Proc. Natl. Acad. Sci. U.S.A. 92*, 8861−8865.
4. Hsiang, Y.-H., Hertzberg, R., Hecht, S., and Liu, L. F. (1985) *J. Biol. Chem. 260*, 14873−14878.
5. Hertzberg, R. P., Caranfa, M. J., and Hecht, S. M. (1989) *Biochemistry 28*, 4629−4638.
6. Porter, S. E., and Champoux, J. J. (1989) *Nucleic Acids Res. 17*, 8521−8532.
7. Chen, A. Y., Yu, C., Gatto, B., and Liu, L. F. (1993) *Proc. Natl. Acad. Sci. U.S.A. 90*, 8131−8135.
8. Chen, A. Y., Yu, C., Bodley, A., Peng, L. F., and Liu, L. F. (1993) *Cancer Res. 53*, 1332−1337.
9. Sun, Q., Gatto, B., Yu, C., Liu, A., Liu, L. F., and LaVoie, E. J. (1994) *Bioorg. Med. Chem. Lett. 4*, 2871−2876.
10. Kim, J. S., Gatto, B., Yu, C., Liu, A., Liu, L. F., and LaVoie, E. J. (1996) *J. Med. Chem. 39*, 992−998.
11. Sun, Q., Gatto, B., Yu, C., Liu, A., Liu, L. F., and LaVoie, E. J. (1995) *J. Med. Chem. 38*, 3638−3644.
12. Pjura, P. E., Grzeskowiak, K., and Dickerson, R. E. (1987) *J. Mol. Biol. 197*, 257−271.
13. Spink, N., Brown, D. G., Skelly, J. V., and Neidle, S. (1994) *Nucleic Acids Res. 22*, 1607−1612.
14. Teng, M.-K., Usman, N., Frederick, C. A., and Wang, A. H.-J. (1988) *Nucleic Acids Res. 16*, 2671−2690.
15. Vega, M. C., García Sáez, I., Aymamí, J., Eritja, R., Van Der Marel, G. A., Van Boom, J. H., Rich, A., and Coll, M. (1994) *Eur. J. Biochem. 222*, 721−726.
16. Clark, G. R., Gray, E. J., Neidle, S., Li, Y.-H., and Leupin, W. (1996) *Biochemistry 35*, 13745−13752.
17. Parkinson, J. A., Barber, J., Douglas, K. T., Rosamond, J., and Sharples, D. (1990) *Biochemistry 29*, 10181−10190.
18. Fede, A., Labhardt, A., Bannwarth, W., and Leupin, W. (1991) *Biochemistry 30*, 11377−11388.
19. Fede, A., Billeter, M., Leupin, W., and Wüthrich, K. (1993) *Structure 1*, 177−186.
20. Pilch, D. S., Xu, Z., Sun, Q., LaVoie, E. J., Liu, L. F., Geacintov, N. E., and Breslauer, K. J. (1996) *Drug Des. Discuss. 13* (3−4), 115−133.
21. Gatto, B., Sanders, M. M., Yu, C., Wu, H.-Y., Makhey, D., LaVoie, E. J., and Liu, L. F. (1996) *Cancer Res. 56*, 2795−2800.
22. Griswold, B. L., Humoller, F. L., and McIntyre, A. R. (1951) *Anal. Chem. 23*, 192−194.
23. Bodley, A. L., Liu, L. F., Israel, M., Ramakrishnan, S., Yoshihiro, K., Giuliani, F. C., Kirschenbaum, S., Silber, R., and Potmesil, M. (1989) *Cancer Res. 49*, 5969−5978.
24. Christianson, T. W., Sikorski, R. S., Dante, M., Shero, J. H., and Hieter, P. (1992) *Gene 110*, 119−122.
25. Marky, L. A., and Breslauer, K. J. (1987) *Biopolymers 26*, 1601−1620.
26. Geacintov, N. E., Ibanez, V., Rougée, M., and Bensasson, R. V. (1987) *Biochemistry 26*, 3087−3092.
27. Mudd, C. P., and Berger, R. L. (1988) *J. Biochem. Biophys. Methods 17*, 171−192.
28. Remeta, D. P., Mudd, C. P., Berger, R. L., and Breslauer, K. J. (1991) *Biochemistry 30*, 9799−9809.
29. Robinson, A. L. (1932) *J. Am. Chem. Soc. 54*, 1311−1318.
30. Gulbransen, E. A., and Robinson, A. L. (1934) *J. Am. Chem. Soc. 56*, 2637−2641.
31. Nordén, B. (1978) *Appl. Spectrosc. Rev. 14*, 157−248.
32. Nordén, B., Kubista, M., and Kurucsev, T. (1992) *Q. Rev. Biophys. 25*, 51−170.
33. Wilson, R. W., and Schellman, J. A. (1978) *Biopolymers 17*, 1235−1248.
34. Geacintov, N. E., Gagliano, A., Ivanovic, V., and Weinstein, I. B. (1978) *Biochemistry 17*, 5256−5262.
35. Pilch, D. S., Xu, Z., Sun, Q., LaVoie, E. J., Liu, L. F., and Breslauer, K. J. (1997) *Proc. Natl. Acad. Sci. U.S.A. 94*, 13565−13570.
36. Crothers, D. M. (1971) *Biopolymers 10*, 2147−2160.
37. Snyder, J. G., Hartman, N. G., D'Estantoit, B. L., Kennard, O., Remeta, D. P., and Breslauer, K. J. (1989) *Proc. Natl. Acad. Sci. U.S.A. 86*, 3968−3972.

38. Chou, W. Y., Marky, L. A., Zaunczkowski, D., and Breslauer, K. J. (1987) *J. Biomol. Struct. Dyn. 5*, 345−359.
39. Breslauer, K. J., Freire, E., and Straume, M. (1992) *Methods Enzymol. 211*, 533−567.
40. Pilch, D. S., Kirolos, M. A., Liu, X., Plum, G. E., and Breslauer, K. J. (1995) *Biochemistry 34*, 9962−9976.
41. Pilch, D. S., Poklar, N., Gelfand, C. A., Law, S. M., Breslauer, K. J., Baird, E. E., and Dervan, P. B. (1996) *Proc. Natl. Acad. Sci. U.S.A. 93*, 8306−8311.
42. Pilch, D. S., Yu, C., Makhey, D., LaVoie, E. J., Srinivasan, A. R., Olson, W. K., Sauers, R. R., Breslauer, K. J., Geacintov, N. E., and Liu, L. F. (1997) *Biochemistry 36*, 12542−12553.
43. Caserta, M., Amadei, A., Mauro, E. D., and Camilloni, G. (1989) *Nucleic Acids Res. 17*, 8463−8474.
44. Krogh, S., Mortensen, U. H., Westergaard, O., and Bonven, B. J. (1991) *Nucleic Acids Res. 19*, 1235−1241.

BI9727747